J Appl Electrochem (2014) 44:169–177
DOI 10.1007/s10800-013-0623-5

RESEARCH ARTICLE

The reduction of hydrogen peroxide at an Au-coated nanotubular TiO_2 array

C. T. J. Low · C. Ponce de Leon · F. C. Walsh

Received: 4 July 2013 / Accepted: 2 September 2013 / Published online: 1 October 2013

Abstract An Au-coated TiO_2 nanotubular array, in the vertically aligned form, was investigated as a highly porous nanostructured electrode for the electrochemical reduction of H_2O_2 in an acidic sulphate electrolyte at 295 K. The TiO_2 nanotubular arrays were formed via a two-stage anodising then nanosized Au particles were sputter deposited onto the surface. The following aspects were studied: (a) the shape evolution of Au particles on the nanotubular array (via surface microstructural imaging), (b) the effect of different degrees of Au loading on the nanotubular array (via voltammetric analysis) and (c) the electrochemical response of an Au–TiO_2 nanotubular array compared to a plain, 2-D Au foil. The Au particles could be deposited as a thin 3-D coated layer or as nodular nanostructures on the array. The highly nanoporous structure of the Au–TiO_2 electrode led to a large enhancement in the limiting current (enhancement factor up to 6.6) and charge density (enhancement factor up to 8.9) for peroxide reduction compared to a plain Au foil due to the architecture of the ordered, high surface area of the nanotubular array.

Keywords Anodising · Electrocatalyst · Gold · Nanostructure · Nanotubular array · Peroxide reduction · Titanium oxide · Nanotubes · Three-dimensional

C. T. J. Low · C. Ponce de Leon (✉) · F. C. Walsh
Electrochemical Engineering Laboratory, Energy Technologies Group, University of Southampton, Highfield, Southampton SO17 1BJ, UK
e-mail: capla@soton.ac.uk

Present Address:
C. T. J. Low
WMG, School of Engineering, University of Warwick, Coventry CV4 7AL, UK

1 Introduction

The electrochemical reduction of the liquid fuel hydrogen peroxide (H_2O_2), is an important reaction for the development of future energy conversion technology. This reaction has been investigated as an alternative to oxygen reduction in air-powered batteries and fuel cells, where the supply of oxygen (or air from the surrounding atmosphere) is not readily available (e.g. in space and underwater). Examples of H_2O_2 powered fuel cell may include various types of anodic reactions such as (a) a metal-based system, e.g. Al–H_2O_2 [1] and Mg–H_2O_2 [2], or (b) a liquid-based system, e.g. CH_3OH–H_2O_2 [3] and $NaBH_4$–H_2O_2 [4].

H_2O_2 can be an attractive choice to replace compressed air or liquid oxygen as an oxidant for batteries and fuel cells working in environments without air. The reasons include: (a) the electrochemical reduction of H_2O_2 is a two-electron transfer process having a lower activation energy than the 4-electron oxygen reduction reaction; (b) H_2O_2 is liquid at standard conditions and much denser than a gas phase oxidant; its handling, storage and delivery into the cell do not require complicated processes and its engineering design is easy to achieve a higher energy density and compact structural design. The increasingly popular use of H_2O_2 has also been driven by a recent price drop, industrial scale manufacturing and the reagents green environmental credentials as the only waste products are oxygen (via catalytic decomposition), or water or hydroxyl ions (via electrochemical reduction).

The rate of electrochemical reduction of hydrogen peroxide to water (in acidic conditions) or to hydroxyl ions (in alkaline or neutral conditions) is a major factor determining the performance of hydrogen peroxide powered batteries and fuel cells. The challenge, to-date, have been to enhance the electrocatalysts properties towards a more efficient

electrochemical reduction of H_2O_2. Two main approaches have been deployed, namely (a) design of new and improved electrocatalysts to be more electroactive and longer lasting and (b) the deliberate architecture of a higher surface area electrocatalysts to increase the power density.

Au is one of the few suitable materials [5, 6] and can slow down the spontaneous catalytic decomposition of H_2O_2. It has a high oxidation potential ca. $E = +1.498$ V versus SHE; is stable at high oxidation potentials and is corrosion resistant. Au can be prepared in several forms, including nanoplates for the amperometric detection of H_2O_2 at micro molar levels [7] or as nanoparticles coated onto conductive micron-sized particles, e.g. carbon, then pasted onto a conductive substrate, with the help of binders and organic solvents, e.g. Nafion or PTFE, to form a porous electrocatalyst-polymer electrode. The porosity within such a structure is randomly distributed and accessibility to the liquid electrolyte can be limited. The use of non-conductive binders could also reduce the electrical conductivity of the electrode.

To overcome these limitations, nanosized particles of Au coated onto a TiO_2 nanotubular array, in the vertically aligned form, have been used as a novel electrode structure and for the efficient electrochemical reduction of H_2O_2. Manufacture of this type of electrode layer: metal–metal oxide–metal, i.e. Au–TiO_2–Ti removes the need of binders; since it is shown that gold can be sputter deposited directly onto a titanium dioxide nanotubular array which acts as a semiconductive layer; the electrically conductive and chemically inert titanium substrate also acts as a good electrode current feeder. The TiO_2 nanotubular arrays are formed via a two-stage anodising procedure. We compare the electrochemical response of Au–TiO_2 nanotubular arrays with a plain Au thin foil to illustrate the advantageous of the nanoporous and 3-D nanostructured electrode. Voltammograms are obtained for different degrees of Au loading on nanotubular array. It is shown that the enhancement factor is due to a controlled architecture of the ordered, high surface area, nanotubular array.

2 Experimental details

2.1 Chemicals and electrodes

Glycerol (99 %), ammonium fluoride (98 %), hydrogen peroxide (30 %) and sulphuric acid (99 %) were purchased from Sigma Aldrich, UK. Titanium foil (0.25 mm thick, annealed, 95 %) was obtained from Alfa Aesar, UK. Stainless steel plate (2.00 mm thick, SS430, 18/8) was provided by Corus GmbH, Germany. The dimension of the electrodes was 1.0×4.0 cm^2. All chemicals were used in 'as-received' condition. Both electrodes were washed with ethanol then cleaned in an ultrasonic bath with copious amounts of distilled water before use. Gold foil (99.95 % purity, 100 µm thickness) was purchased from Goodfellow Cambridge Ltd., UK; it was degreased with ethanol before use.

2.2 Anodising at a constant cell voltage

A beaker-type cell (volume: 100 mL) was used for all constant cell voltage anodising experiments. The planar titanium foil anode and stainless steel cathode were placed parallel facing each other with a gap 5 mm. The cell voltage was provided using an external power supply (TTi-CPX400A, 60 V, 20 mA, Thurnby Thunder Instruments, UK). The temperature of the electrolyte was 273 ± 2 K. A two-stage anodising was used. The first stage was performed at 30 or 60 V for 24 h then the 'as-formed' TiO_2 nanotubular array was removed via sticky tape. This gave a clean and regularly ordered substrate for the second anodising step. The second anodising was performed at 30 or 60 V for 30 or 120 min. The resultant nanotubular arrays were used in all studies.

2.3 Analysis of surface microstructure

All samples was analysed in the 'as-anodised' condition, either with or without Au-coated surface. Surface microstructural characterisation was carried out using a high resolution scanning electron microscopy (JEOL JSM 6500F). An accelerating voltage of 10 kV was used and the imaging was carried out with a working distance of 10 mm.

2.4 Sputter deposition of gold particles

Gold, Au was sputter deposited onto the surface of the TiO_2 nanotubular array using Hummer 6.2 (Supplier: Anatech Ltd. Serial number: 1029001) and the beam current was 15 mA. The distance between the gold sputter target and the samples was ~ 5 cm. The deposition time ranged from 2 to 30 min. The loading of Au on the TiO_2 nanotubular array was estimated via a high precision balance.

2.5 Electrochemical measurement of hydrogen peroxide reduction

Linear sweep voltammetry response of the samples in 1.0 mol dm^{-2} H_2O_2 and 1.0 mol dm^{-3} H_2SO_4 electrolyte was carried out in an undivided three-electrode glass cell (50 dm^3). The electrolyte temperature was maintained at 273 ± 2 K. The working electrode was the sample with 2.01 cm^2 geometrical area. The counter electrode was a Pt mesh of 1 cm^2 area. An Ag|AgCl (3.5 mol dm^{-3} KCl) was

used as the reference electrode. The electrode potential was linearly swept from −0.4 V to −1.0 V versus Ag|AgCl. The potential sweep rate used range from 4 to 512 mV s^{-1}. A computer-controlled potentiostat (EcoChemie Autolab, PGSTAT20) using the General Purpose Electrochemical Software (GPES) Version 4.5 was used.

3 Results and discussion

3.1 Linear sweep voltammograms of H_2O_2 reduction on Au–TiO_2 nanotubular array

Figure 1a shows the linear sweep voltammetry response of Au–TiO_2 nanotubular array in a solution containing 1.0 mol dm^{-3} H_2O_2 and 1.0 mol dm^{-3} H_2SO_4 at 293 K. The electrode potential was linearly swept from +0.4 to −0.8 V versus Ag|AgCl at 5 mV s^{-1}. The nanotubular array was formed at 30 V and 24 h for the first anodising and was removed via a sticky tape. The second anodising was performed at 30 V and 2 h to give regularly ordered and vertically aligned nanotubular array, as confirmed by surface microstructural imaging. These anodising steps and the formation of a nanotubular array followed typical results reported in the literature [8–12].

It is clearly seen that the current density-potential curve in Fig. 1a has a distinct charge transfer, a mixed control zone and a well-defined mass transport controlled region. At a more electronegative potential, the current rose sharply due to hydrogen evolution reaction. The limiting current density was found to be at approximately −8.4 mA cm^{-2} and was estimated at an electrode potential of −0.5 V versus Ag|AgCl. The limiting current shows clear evidence of a single step, two-electron transfer for the cathodic reduction of H_2O_2 to H_2O on the Au–TiO_2 nanotubular array [13]:

$$H_2O_2 + 2H^+ + 2e^- \rightarrow 2H_2O, \quad E^o = 1.776 \text{ versus SHE} \tag{1}$$

H_2O_2 can also spontaneously decompose to produce H_2O and O_2:

$$2H_2O_2 \rightarrow 2H_2O + O_2 \tag{2}$$

for comparison, the voltammetric response of an Au–TiO_2 sample in 1.0 mol dm^{-3} H_2SO_4 solution in the absence of H_2O_2 was studied. Figure 1b shows a higher magnification of the curves. In the 'as-prepared' solution, two well-defined limiting current plateaux were seen. The fist limiting current was approximately −0.01 mA cm^{-2} while the second was ca. 0.05 mA cm^{-2}; these values were estimated at −0.1 V versus Ag|AgCl and −0.3 V versus Ag|AgCl, respectively. These plateaux correspond to the electrochemical reductions of, firstly, dissolved oxygen to hydrogen peroxide then hydrogen peroxide to water [14, 15]:

$$O_2 + 2H^+ + 2e^- \rightarrow H_2O_2, \quad E^o = 0.695 \text{ versus SHE} \tag{3}$$

$$H_2O_2 + 2H^+ + 2e^- \rightarrow 2H_2O \tag{1}$$

It was found that the cathodic current rose abruptly at the end of the first step reduction reaction from oxygen to hydrogen peroxide, which may suggest a fast complete conversion of hydrogen peroxide to water at the nanotubular array. To further illustrate these two reduction steps, the solution containing no peroxide was bubbled with oxygen for 10 min and linear sweep voltammogram are recorded. The voltammetric response

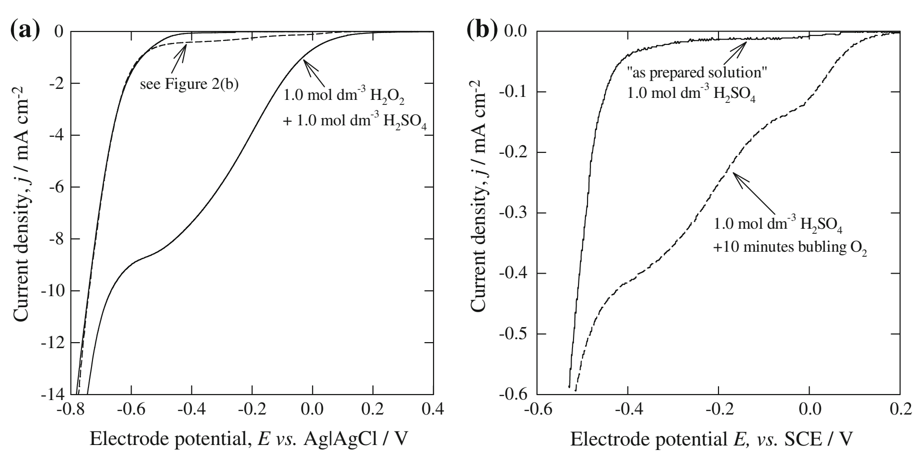

Fig. 1 Linear sweep voltammograms of an Au-coated TiO_2 nanotubular array in **a** a solution containing 1.0 mol dm^{-3} H_2O_2 and 1.0 mol dm^{-3} H_2SO_4 at 293 K. The electrode had a loading of 78 µg cm^{-2} Au. The electrode potential was linearly swept from +0.4 to −0.8 V versus Ag|AgCl at 5 mV s^{-1}. **b** Shows a higher magnification of the Au–TiO_2 nanotubular array in 1.0 mol dm^{-3} H_2SO_4 in the absence of H_2O_2, showing the response recorded in an as-prepared solution and one which had been O_2 saturated

clearly shows an increase in the limiting currents; as-predicted since the solution contained a higher concentration of dissolved oxygen. These results illustrate that the Au–TiO_2 nanotubular array is an active electrode surface for the reduction of O_2 and H_2O_2. The recorded currents in an electrolyte containing no peroxide are significantly lower than that reported for an electrolyte containing peroxide. An efficient O_2 reduction electrode would involve a single step, four electron transfer of oxygen reduction to water [16]:

$$O_2 + 4H^+ + 4e^- \rightarrow 2H_2O, \quad E^o = 1.229 \text{ versus SHE.} \tag{4}$$

3.1.1 *The shape evolution of nanosized Au particles coated onto the TiO_2 nanotubular array*

It is well known that the size and shape of Au particles can affect the electrochemical kinetics of oxygen and hydrogen peroxide reductions [17, 18]. Therefore, we have investigated the shape evolution of Au particles formed on the TiO_2 nanotubular array. The TiO_2 nanotubular array were gold sputter coated at various deposition times (from 2 to 30 min) to give a controlled degree of Au loading (from 38 to 179 μg cm^{-2}) on the array.

Figure 2 shows the gradual development of surface microstructures of Au–TiO_2 nanotubular array. Figure 2b shows the 'as-formed' TiO_2 nanotubular array; first anodised at 60 V for 24 h and then second anodised at 60 V for 30 min. Regularly distributed open pores on the top surface of the nanotubular array were again imaged. The nanotubular array showed all the essential features (structural and physical) of an anodised titanium foil, including uniform pore size: 100–200 nm and wall thickness: 100–200 nm. The inset shows the back view of nanotubular array. The nanotubular array was formed via: first anodising at 60 V for 24 h followed by a second anodising at 60 V for 2 h. It is clearly seen that the nanotubular array had a closed cup, rounded bottom and was vertically aligned on the titanium substrate. The nanotubular array had an inner diameter of ca. 150 nm, a wall thickness 100–200 nm and a tube length of 300 nm. The prepared samples appeared purple after anodising for 30 min; and pale, grey white after the second anodising for 2 h. This observation is expected since longer tubes were formed at a longer anodising time affect the surface reflectivity of the sample [19, 20].

Figure 2c, d shows the surface microstructures of different degrees of Au loading on the TiO_2 nanotubular array; and also shows mutually parallel pores arranged in a hexagonally array with a pitch of ca. 300 nm. The deposited Au particles had several to tens of nanometre dimensions. It was found that the shape and size of the Au particles changed as a function of Au deposition time; probably associated with nucleation of deposit and its subsequent growth on the nanotubular array. Since the sputter deposition method is a 'line-of-sight' process, Au particles only deposited along the side wall and on the exposed surface on the nanotubular array, i.e. inner tube bottoms, tube walls and open-mouth top surface of the tubes.

After several minutes Au deposition time, e.g. <10 min, the Au particles appeared to be deposited as a thin film layer uniformly coated onto the walls of the nanotubular array as shown in Fig. 2c. The inset shows a higher magnification of the microstructure and clearly shows the nanotubular array retained ca. 120 nm inner pore diameters. After a 10 min deposition time, this Au coating layer appeared as slightly roughened microstructure; see Fig. 2d. The inset shows a tilted view of the sample (both front side and back side of the nanotubular array); clearly indicates that the Au nanosized particles ca. 50 nm diameter deposited vertically on the top surface of the nanotubular array. At an even longer deposition time, e.g. 20 and 30 min, a nodular, porous Au layer can be seen in Fig. 2e.

A pictorial representation of this shape evolution process is shown in Fig. 2a. Over all the deposition times investigated, the Au was deposited as nanosized particles. For example, the diameter of nodular Au particles changed from 50 to 100 nm, over 20 and 30 min deposition time, respectively. The nanosized Au particles grew on top of each other instead of over-covering the hollow space within the tube. It was also found that at increasing deposition times: (a) the wall of the nanotubular array became thicker, (b) the inner diameter of the nanotubular array became narrower and (c) the pore mouth became narrower. In all the samples tested, the Au-coated nanotubular array structure remained open porous, i.e. the top mouth of the nanotubular array remained unblock by the deposited Au particles, which is an important feature to retain its high surface area characteristic. This unique nanoporous microstructure differs from the microstructures typically reported for a previous Au-coated TiO_2 nanotubular array; where a high loading of Au particles can overfill the nanotubular array and block the inner tube spacing [21, 22].

3.2 Comparison of an Au–TiO_2 nanotubular array with an Au foil

To illustrate the benefit of this controlled architecture of an Au–TiO_2 nanotubular array as an electrode for the reduction of H_2O_2. Figure 3 compares the linear sweep voltammograms with a plain Au foil in (a) and an Au–TiO_2 nanotubular array in (b). The Au–TiO_2 nanotubular array showed a well-defined charge transfer controlled zone, a mixed controlled zone and a mass transport controlled one.

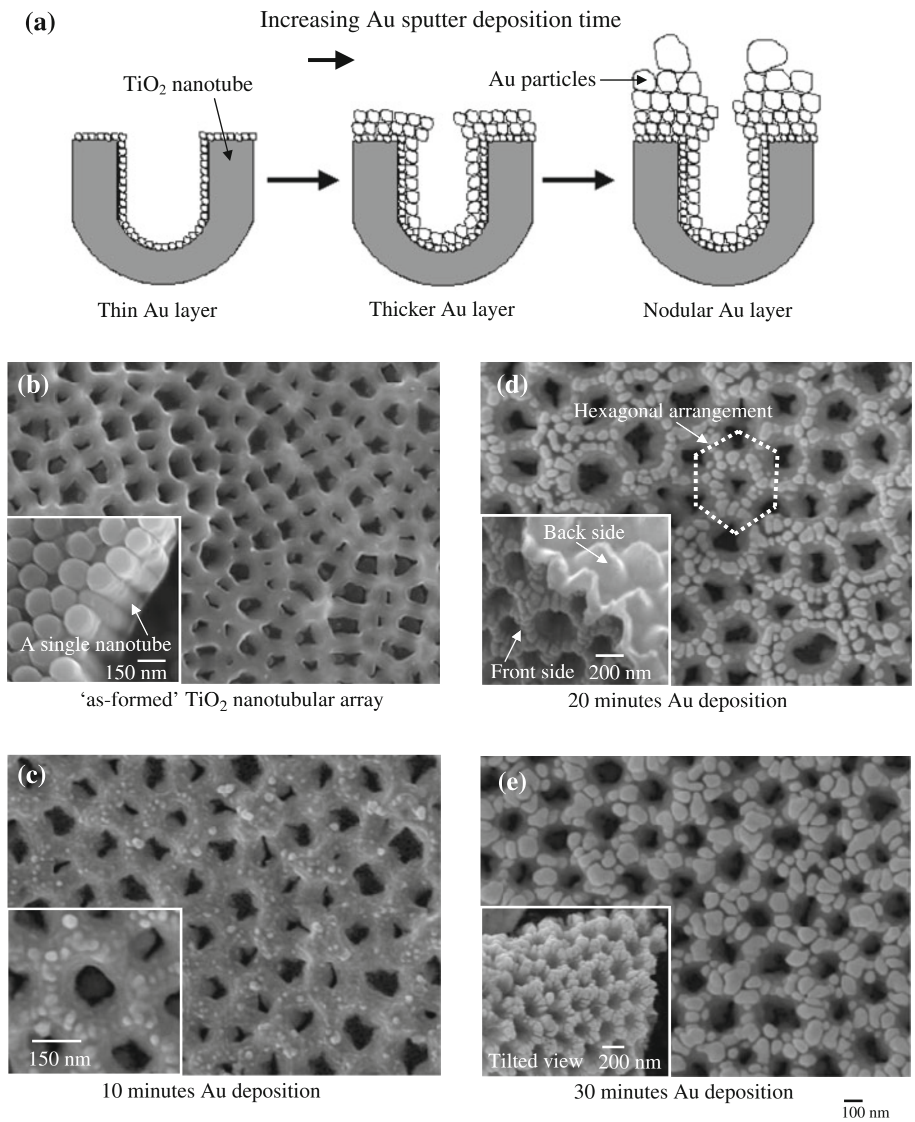

Fig. 2 Surface microstructure of Au-coated TiO_2 nanotubular arrays, showing a gradual development in the shape evolution of Au nanosized particles. **a** A schematic representation of the Au-deposits on TiO_2 nanotubular array, **b** as-formed TiO_2 nanotubular array via anodising on a titanium foil, **c** 10 min Au deposition; corresponded to $\sim$69 µg cm^{-2} Au on TiO_2, **d** 20 min Au deposition; 164 µg cm^{-2} Au on TiO_2 and **e** 30 min Au deposition; 179 µg cm^{-2} Au on TiO_2

The curves retained a characteristic single step, two-electron transfer for peroxide reduction at various electrode potential sweep rates. At an increasing potential sweep rate, the following were observed (a) the mass transport controlled region became narrower, (b) the mixed controlled region was lengthened and (c) the electrode potential for onset of hydrogen evolution shifted to a more negative potential.

In the absence of the porous nanostructured geometry, the plain Au foil did not show an obvious limiting current plateau; and this observation is more clearly demonstrated at a high potential sweep rate and a steady increase in the current towards the hydrogen evolution reaction. For comparison, the current recorded on the Au–TiO_2 nanotubular array was found to be higher than the one recorded on the Au foil at a similar overpotential. This shows the nanotubular array structure is effective for high current applications; since the limiting current for peroxide reduction remained clearly defined at fast potential sweep rates, e.g. 512 mV s^{-1} showing that the Au–TiO_2 nanotubular array demonstrates a fast response and could find applications in high speed energy conversion technology. The architecture of the nanotubular array facilitated high rates of peroxide diffusion down the vertically aligned pores perpendicular to the electrode surface.

Figure 3c shows the peak current density for peroxide reduction had a linear correlation with the square root of electrode potential sweep rate. This suggested that the peroxide reduction is a diffusion-controlled reaction and consistent with the Randles–Sevcik relationship [23, 24]. The figure shows that the peak current values were dependent on the degrees of Au loading on TiO_2 nanotubular array. It was also found that the speed of the electrode potential sweep rate had an effect on its electrochemical

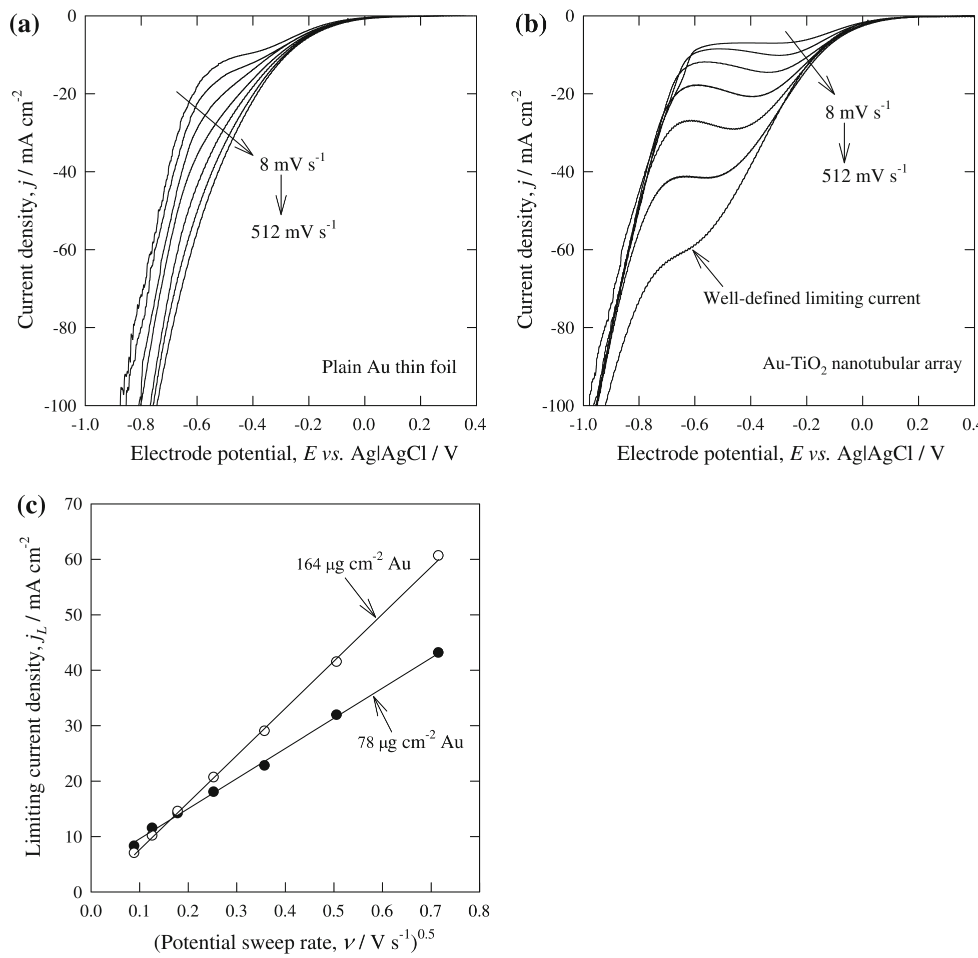

Fig. 3 Comparison of the linear sweep voltammograms recorded for **a** a thin Au foil and **b** a Au–TiO_2 nanotubular array; the electrode was loaded with 78 μg cm^{-2} Au on TiO_2. The solution contained 1.0 mol dm^{-3} H_2O_2 and 1.0 mol dm^{-3} H_2SO_4 at 293 K. The electrode potential was linearly swept from +0.4 to −1.0 V versus Ag|AgCl at a range of speed ca. 8, 16, 32, 64, 128, 256 and 512 mV s^{-1}. **c** Peak current density, i.e. on the reduction of H_2O_2 versus square root of electrode potential sweep rate; comparing the effect of two Au loadings on the peak current values

response. At slow potential sweep rates, e.g. 8 and 16 mV s^{-1}, the recorded limiting currents were slightly higher in 78 μg cm^{-2} Au–TiO_2 sample as compared with 164 μg cm^{-2} Au–TiO_2 sample. For example, the peak current was 8.2 mA cm^{-2} for 79 μg cm^{-2} Au–TiO_2 and 6.9 mA cm^{-2} for 164 μg cm^{-2} Au–TiO_2, which does not follow the usual expectation that peak current increases at a higher degree of Au loading. Higher potential sweep rates, e.g. from 32 mV s^{-1} upwards, the recorded limiting currents were as-expected to become higher as more Au was coated onto the TiO_2 nanotubular array. For example, at 64 mV s^{-1} potential sweep rate, the peak current was 18.2 mA cm^{-2} for 79 μg cm^{-2} Au–TiO_2 compared to 20.6 mA cm^{-2} for 164 μg cm^{-2} Au–TiO_2, which follows the normal trend.

3.3 Comparison of voltammograms for peroxide reduction on different samples

Figure 4 shows the linear sweep voltammograms at a very slow potential sweep rate, e.g. 4 mV s^{-1}, recorded for a number of different electrodes, including a plain Au foil (dotted line), an 'as-formed' TiO_2 nanotubular array (i.e. not coated with Au particles) and three samples of Au-coated TiO_2 nanotubular array.

The 'as-formed' TiO_2 nanotubular array required the most electronegative potential for the reduction of H_2O_2; which is as-expected since TiO_2 is not particularly active as an electrocatalyst for peroxide reduction. For samples Au–TiO_2 nanotubular array, the onset potential where the cathodic current started to rise is significantly more positive than the 'as-formed' nanotubular array. This trend is as-expected since Au is an effective electrocatalyst for peroxide reduction; thus less overpotential was required for peroxide reduction reaction on the Au-TiO_2 nanotubular array. In all these nanotubular array samples, the mixed controlled region occupied a wide range of potential window; and the mass transport controlled region was demonstrated in a narrow range of potential window. This could be attributed to the nature of diffusion phenomenon inside a confined nanotubular structure where water, the reaction product, could be slowly flooding the open-space in the nanotubes.

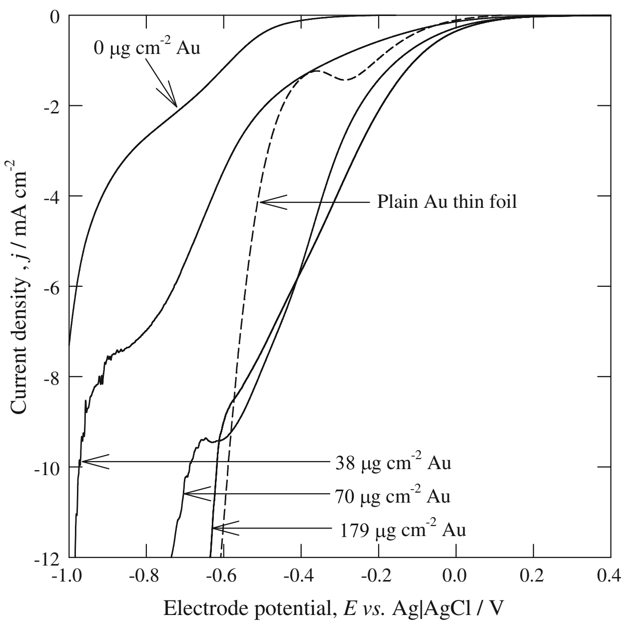

Fig. 4 The effect of different degrees of Au loading on the TiO_2 nanotubular array on the linear sweep voltammograms recorded in 1.0 mol dm^{-3} H_2O_2 and 1.0 mol dm^{-3} H_2SO_4 at 293 K. The electrode potential was linearly swept from +0.4 to −1.0 V versus Ag|AgCl at 4 mV s^{-1}. The *dotted line* shows the response recorded for an Au foil under similar conditions

Several features on the voltammograms can be seen when a higher degree of Au was coated onto TiO_2 nanotubular array: (a) the voltammograms shifted to a more positive potential direction with respect to an increasing amount of Au loaded onto the array, (b) the recorded limiting current density for Au–TiO_2 nanotubular array is several times higher than that of a plain Au foil, see Table 1 and (c) a narrow mass transport controlled region was recorded before a sharp rise in the cathodic current for hydrogen evolution. Table 1 shows the estimated limiting current density and the coulombic density for the reduction of peroxide; comparing the values for a plain Au foil with different degrees of Au loading on the TiO_2 nanotubular array.

The cathodic limiting current and charge density were clearly enhanced in the presence of a nano-architecture tubular structure; see the enhancement factor values in Table 1. The highest values were found on a sample containing 70 μg cm^{-2} Au–TiO_2; enhancement factor ca. 6.6 based on the estimation of limiting current density and enhancement factor of ~8.9 based on the estimation of charge density. However, the increase in these values is not linear with an increase in the Au loading. For example, the limiting current density was 7.38 mA cm^{-2} on a 38 μg cm^{-2} Au–TiO_2 sample (ca. 2 min Au deposition); but it was 9.45 mA cm^{-2} on a 70 μg cm^{-2} Au–TiO_2 sample (ca. 5 min Au deposition). At 179 μg cm^{-2} Au loading (ca. 30 min Au deposition), the limiting current density dropped to 8.6 mA cm^{-2}. This trend is similar for the calculated coulombic density.

A reduction in the limiting current density and coulombic density at a higher Au loading could be attributed to a reduced active surface area available for peroxide reduction. This is supported by the surface microstructure images shown in Fig. 2b–e; where the nanotubular array was steadily filled up with Au particles and they were evidently overlapped and became more nodular at a higher degree of Au loading on the nanotubular array. The nature of diffusion layer on the nano-structures could also contribute to this observation; in which (a) at a low Au loading, the diffusion layer would have followed the shape of the nanostructure since only a thin layer of Au covered the nanotubular array, and (b) at a high Au loading, the diffusion layer would have followed a macro-profile due to the presence of larger-sized Au particles. We also found that the Au loading had an effect on the physical stability of the electrode. For example, on a sample containing 38 μg cm^{-2} Au–TiO_2, the nanostructure layer delaminated from the titanium substrate due to a vigorous gaseous evolution during operation. However, at 179 μg cm^{-2} Au–

Table 1 Limiting current density and calculated charge density for the reduction of peroxide at electrodes having a geometrical area of 1 cm^2 in 1.0 mol dm^{-3} H_2O_2 plus 1.0 mol dm^{-3} H_2SO_4 at 293 K, showing the importance of gold loading hence sputter deposition time

Type of Au substrate	Limiting current density (mA cm^{-2})	Charge density (mC cm^{-2})	Enhancement factor	
			Limiting current density Au–TiO_2 nanotubular array divided by that at an Au foil	Charge density Au–TiO_2 nanotubular array divided by that at an Au foil
Au foil	1.43	81.5	1	1
Au-sputtered TiO_2 nanotubular array/μg cm^{-2} Au				
0	2.45	207.2	1.7	2.5
38	7.38	601.4	5.2	7.4
70	9.45	731.1	6.6	9.0
179	8.85	559.8	6.2	6.9

TiO_2, the nanostructure layer remained intact to the titanium substrate and its adhesion may be further improved by annealing.

4 Conclusions

A nanostructured electrode layer consisting of metal–metal oxide–metal, i.e., Au nanoparticles on a nanotubular TiO_2 array on a thin Ti foil was produced. This electrically conductive layer on a chemically inert titanium substrate was investigated as an electrocatalytically active electrode material for the electrochemical reduction of H_2O_2 in an acidic environment (1.0 mol dm^{-3} H_2SO_4 and 1.0 mol dm^{-3} H_2O_2 at 293 K). This orderly nanoporous, 3-D nanostructured and vertically aligned electrode was readily formed via a two-stage anodising followed by a sputter deposition overcoat.

Various Au loadings (up to 179 μg cm^{-2}) were investigated; The electrode structure could support a single step, two-electron transfer peroxide reduction to water and showed a well-defined mass transport controlled region in linear sweep voltammetry. The peroxide reduction on these nanotubular arrays was diffusion controlled as supported by the linear relationship in the peak current density versus square root of potential sweep rate plot. The recorded limiting current was in the range of several up to tens of milliampere per centimetre; and the mass transport zone remained well defined even at high potential sweep rates (4–512 mV s^{-1}).

The Au nanosized particles deposited on the TiO_2 nanotubular array were found to evolve in shape and size at different Au loadings (2–30 min Au deposition duration); where it evolved as a thin film 3-D coated layer to become a nodular nanostructure on the TiO_2 nanotubular array. This deliberate, controlled architecture of a highly nanoporous, nanotubular array electrode structure had an improvement in electrochemical properties for H_2O_2 reduction compared to a plain thin Au foil; the enhancement in the limiting current density (by factor up to 6.6) and charge density (by a factor of up to 8.9) were demonstrated.

Acknowledgments Financial support provided by the Research Institute for Industry (RIfI) at Southampton University is gratefully acknowledged.

References

1. Li Q, Bjerrum NJ (2002) Aluminum as anode for energy storage and conversion: a review. J Power Sour 110:1–10. doi:10.1016/S0378-7753(01)01014-X
2. Medeiros MG, Bessette RB, Deschenes CM, Patrissi CJ, Carreiro LG, Tucker SP, Atwater DW (2003) Magnesium-solution phase catholyte semi-fuel cell for undersea vehicles. J Power Sour 136:226–231. doi:10.1016/j.jpowsour.2004.03.024
3. Prater DN, Rusek JJ (2003) Energy density of a methanol/hydrogen-peroxide fuel cell. Appl Energy 74:135–140. doi:10.1016/S0306-2619(02)00139-3
4. Ponce de Leon C, Walsh FC, Rose A, Lakeman JB, Browning DJ, Reeve RW (2007) A direct borohydride-acid peroxide fuel cell. J Power Sour 164:441–448. doi:10.1016/j.jpowsour.2006.10.069
5. Ponce de León C, Merino-Jiménez I, Shah AA, Walsh FC (2012) Developments in direct borohydride fuel cells and remaining challenges. J Power Sour 219:339–357. doi:10.1016/j.jpowsour.2012.06.091
6. Cao D, Gao Y, Wang G, Miao R, Liu Y (2010) A direct $NaBH_4$–H_2O_2 fuel cell using Ni foam supported Au nanoparticles as electrodes. Int J Hydrogen Energy 35:807–813. doi:10.1016/j.ijhydene.2009.11.026
7. Ning R, Lu W, Zhang Y, Qin X, Luo Y, Hu J, Asiri AM, Al-Youbi AO, Sun X (2012) A novel strategy to synthesize Au nanoplates and their application for enzymeless H_2O_2 detection. Electrochim Acta 60:13–16. doi:10.1016/j.electacta.2011.10.066
8. Sarapuu A, Tammeveski K, Tenno TT, Sammelselg V, Kontturi K, Schiffrin DJ (2001) Electrochemical reduction of oxygen on thin-film Au electrodes in acid solution. Electrochem Commun 3:446–450. doi:10.1016/S1388-2481(01)00198-9
9. Shin Y, Lee S (2008) Self-organized regular arrays of anodic TiO_2 nanotubes. Nano Lett 8:3171–3173. doi:10.1021/nl801422w
10. Kim JH, Zhu K, Yan Y, Perkins CL, Frank AJ (2010) Microstructure and pseudocapacitive properties of electrodes constructed of oriented NiO–TiO_2 nanotube arrays. Nano Lett 10:4099–4104. doi:10.1021/nl102203s
11. Wang D, Liu L, Zhang F, Tao K, Pippel E, Domen K (2011) Spontaneous phase and morphology transformations of anodized titania nanotubes induced by water at room temperature. Nano Lett 11:3649–3655. doi:10.1021/nl2015262
12. Mor GK, Shankar K, Paulose M, Varghese OK, Grimes CA (2006) Use of highly-ordered TiO_2 nanotube arrays in dye-sensitized solar cells. Nano Lett 6:215–218. doi:10.1021/nl052099j
13. Ghicov A, Macak JM, Tsuchiya H, Kunze J, Haeublein V, Frey L, Schmuki P (2006) Ion implantation and annealing for an efficient N-doping of TiO_2 nanotubes. Nano Lett 6:1080–1082. doi:10.1021/nl0600979
14. Cao D, Sun L, Wang G, Lv Y, Zhang M (2008) Kinetics of hydrogen peroxide electroreduction on Pd nanoparticles in acidic medium. J Electroanal Chem 621:31–37. doi:10.1016/j.jelechem.2008.04.007
15. Dilimon VS, Narayanan NSV, Sampath S (2010) Electrochemical reduction of oxygen on gold and boron-doped diamond electrodes in ambient temperature, molten acetamide–urea–ammonium nitrate eutectic melt. Electrochim Acta 55:5930–5937. doi:10.1016/j.electacta.2010.05.047
16. Kinoshita K (1992) Electrochemical oxygen technology. Wiley, New York
17. Macak JM, Schmidt-Stein F, Schmuki P (2007) Efficient oxygen reduction on layers of ordered TiO_2 nanotubes loaded with Au nanoparticles. Electrochem Commun 9:1783–1787. doi:10.1016/j.elecom.2007.04.002
18. Inasaki T, Kobayashi S (2009) Particle size effects of gold on the kinetics of the oxygen reduction at chemically prepared Au/C catalysts Original. Electrochim Acta 54:4893–4897. doi:10.1016/j.electacta.2009.02.075
19. El-Deab MS, Ohsaka T (2002) Hydrodynamic voltammetric studies of the oxygen reduction at gold nanoparticles-electrodeposited gold electrodes. Electrochim Acta 47:4255–4261. doi:10.1016/S0013-4686(02)00487-5
20. Low CTJ, de la Toba Corral M, Walsh FC (2011) Anodising of titanium in methanesulphonic acid to form titanium dioxide

nanotube arrays. Trans Inst Met Finish 89:44–50. doi:10.1179/174591911X12953503084903
21. Macak JM, Hildebrand H, Marten-Jahns U, Schmuki P (2008) Mechanistic aspects and growth of large diameter self-organized TiO_2 nanotubes. J Electroanal Chem 621:254–266. doi:10.1016/j.jelechem.2008.01.005
22. Mor GK, Varghese OK, Paulose M, Shankar K, Grimes CA (2006) A review on highly ordered, vertically oriented TiO_2 nanotube arrays: fabrication, material properties, and solar energy applications. Sol Energy Mater Sol Cell 90:2011–2075. doi:10.1016/j.solmat.2006.04.007
23. Macak JM, Tsuchiya H, Ghicov A, Yasuda K, Hahn R, Bauer S, Schmuki P (2007) TiO_2 nanotubes: self-organized electrochemical formation, properties and applications. Curr Opin Solid State Mater Sci 11:3–18. doi:10.1016/j.cossms.2007.08.004
24. Low CTJ, Walsh FC (2008) Linear sweep voltammetry of the electrodeposition of copper from a methanesulfonic acid bath containing a perfluorinated cationic surfactant. Surf Coating Technol 202:3050–3057. doi:10.1016/j.surfcoat.2007.11.005